



1 Implementation and evaluation of open boundary conditions for sea 2 ice in a regional coupled ocean (ROMS 3.7) and sea ice (CICE 5.1.2) 3 modelling system

4
5 Pedro Duarte¹, Jostein Brændshøi², Dmitry Shcherbin¹, Pauline Barras¹, Jon Albretsen³, Yvonne Gusdal²,
6 Nicholas Szapiro², Andreas Martinsen¹, Annette Samuelsen⁴, Jens Boldingh Debernard²

7
8 ¹Norwegian Polar Institute, Fram Centre, Tromsø, Norway

9 ²The Norwegian Meteorological Institute, Oslo, Norway

10 ³Institute of Marine Research, Box 1870 Nordnes, 5817 Bergen, Norway

11 ⁴Nansen Environmental and Remote Sensing Centre, Bergen, Norway

12 *Correspondence to:* Pedro Duarte (pedro.duarte@npolar.no)

13 Abstract

14 The Los Alamos Sea Ice Model (CICE) is used by several Earth System Models where sea ice boundary conditions are not
15 necessary, given their global scope. However, regional and local implementations of sea ice models require boundary
16 conditions describing the time changes of the sea ice and snow being exchanged across the boundaries of the model domain.
17 These boundary conditions include but are not limited to: (i) drift direction and velocity; (ii) concentration; (iii) thickness (of
18 the ice and snow); (iv) thermodynamic conditions (with emphasis on sea ice and snow temperature or enthalpy); (v) salinity.
19 The physical detail of these boundary conditions regarding, for example, the usage of different sea ice size categories or the
20 vertical resolution of thermodynamic properties, must also be taken into account when matching them with the requirements
21 of a specific implementation of a sea ice model. Available satellite products do not include all required fields described above.
22 Therefore, the most straightforward way of getting sea ice boundary conditions is from a larger scale model. The main goal of
23 our study is to describe and evaluate the implementation of time-varying sea ice boundaries in the CICE model using two
24 regional coupled ocean-sea ice models, covering a large part of the Barents Sea and areas around Svalbard: the Barents-2.5
25 km, implemented at the Norwegian Meteorological Institute (MET), and the S4K, implemented at the Norwegian Polar
26 Institute (NPI). We use the TOPAZ4 model and a Pan-Arctic 4 km-resolution model (A4) model to generate the boundary
27 conditions for the sea ice and the ocean. The Barents-2.5 km model is MET Norway's main forecasting model for ocean state
28 and sea ice in the Barents Sea. The S4K model covers a similar domain but it is used mainly for research purposes. Obtained
29 results show significant improvements in the performance of the Barents-2.5 km model after the implementation of the time-
30 varying boundary conditions. The performance of the S4K model in terms of sea ice and snow thickness is comparable to that



31 of the TOPAZ4 system but with more accurate results regarding the oceanic component. The implementation of time-varying
32 boundary conditions described in this study is similar regardless of the CICE versions used in different models.

33 **1 Introduction**

34 The Los Alamos Sea Ice Model (CICE) is managed by the CICE Consortium with an active forum
35 (<https://bb.cgd.ucar.edu/cesm/forums/cice-consortium.146/>) and a git repository (<https://github.com/CICE-Consortium>). It
36 includes two independent packages: CICE and Icepack. Sea ice dynamics is handled by CICE and sea ice columnar processes
37 (thermodynamics and biogeochemistry) are handled by Icepack. Previous versions did not have such a separation, but the code
38 evolved over the last years towards a clear distinction between processes which are mainly horizontal and those that are mainly
39 vertical/columnar. Various (older) versions of the CICE model are still in use by several Earth System Models included in
40 CMIP6 [e.g. CICE 4.1, 5.1 and 5.1.2, see Wei et al., (2020)]. Scientific and technical details about the Los Alamos Sea Ice
41 Model may be found in Hunke et al. (2015), Jeffery et al. (2016) the forum, and the Git repository mentioned above.

42 Global, Arctic or Antarctic wide applications of the CICE model do not require any specific treatment regarding sea ice
43 boundary conditions because the model domain is larger than the areas where sea ice may occur. However, this is not the case
44 of regional implementations of the CICE or any other sea ice model. For such regional cases the past and current versions of
45 CICE include a simple way of dealing with open boundaries, restoring them every time step to the initial ice state or to some
46 predefined value, using a relaxation time scale. In the words of Hunke et al. (2015), this implementation is only intended to
47 “provide the hooks” for more sophisticated treatments. Therefore, the main goal of our study is to describe and evaluate the
48 implementation of sea ice time-varying boundaries in the Los Alamos Sea Ice Model using two regional models: the Barents-
49 2.5 km, implemented at the Norwegian Meteorological Institute (MET), and the S4K, implemented at the Norwegian Polar
50 Institute (NPI). We have chosen to use these two models because, whereas the former is an operational forecasting system,
51 using data assimilation and used for relatively short-term simulations (a few days), the latter is a research tool used for hindcast
52 and forecast longer-term simulations (a few years), without data assimilation, and this allowed us to evaluate the time-varying
53 boundary scheme for different types of models and simulations.

54 **2 Methods**

55 **2.1 Model description**

56 **2.1.1 Barents-2.5 km model**

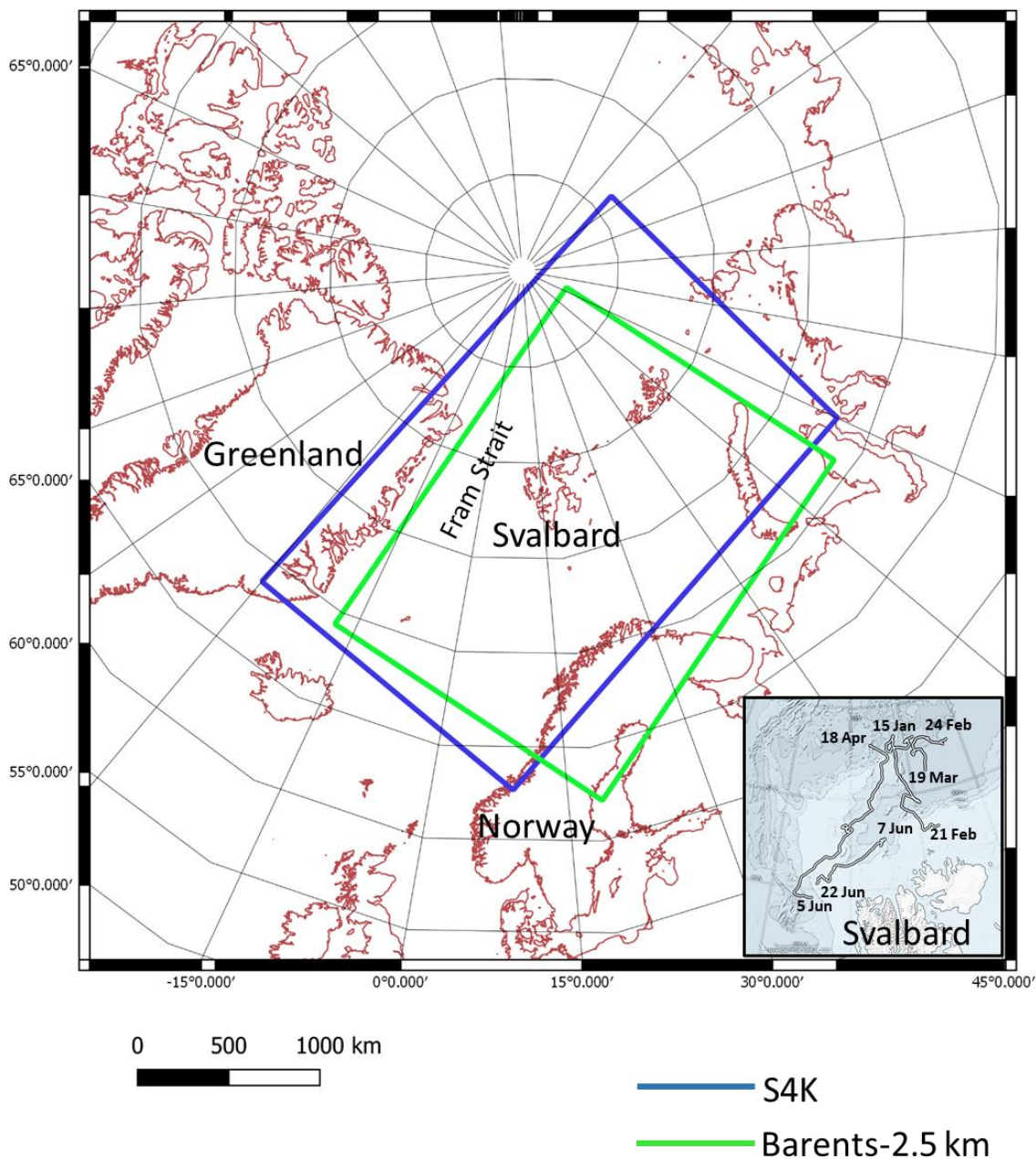
57 The Barents-2.5km model is MET Norway’s primary model for forecasting sea ice conditions in the northern regions. It
58 consists of a fully coupled ocean and sea ice model that covers the Barents Sea and areas around Svalbard (Fig. 1). The



59 modelling system employs the METROMS (<https://doi.org/10.5281/zenodo.5067164>) framework which implements the
60 coupling between the ocean component (Regional Ocean Modeling System, ROMS, <https://www.myroms.org/>) and the sea
61 ice component (The Los Alamos Sea Ice Model, CICE, <https://www.osti.gov/biblio/1364126-cice-los-alamos-sea-ice-model>)
62 (e.g. Fritzner et al., 2019) (for details on coupling refer 2.1.3). The model uses a grid with equally spaced points (2.5 km) in
63 the horizontal, and differentially spaced (42 layers) vertical coordinates following the bathymetry (as is standard with ROMS).
64 The ice is distributed among 5 thickness categories with the lower boundary values: 0.00, 0.64, 1.39, 2.47 and 4.57 m. There
65 are 7 vertical layers and one snow layer for each category. Both the ocean and sea ice utilize atmospheric forcing by AROME-
66 Arctic, MET Norway's own numerical weather prediction model for the Arctic. Considering that this model uses the exact
67 same spatial grid as Barents-2.5km, our ocean and sea ice experience atmospheric forcing without the loss of accuracy through
68 processes like e.g. interpolation. Both ocean and sea ice use boundary conditions from TOPAZ4 (Sakov et al., 2012; Xie,
69 2017). TPXO tidal model is used for tidal input and river runoff climatology is based on NVE data for mainland Norway and
70 AHYPE hydrological model for Svalbard and Russia. The bathymetry is a smoothed version made from the IBCAO v3 dataset.
71 Operationally, the model assimilates AMSR2 sea ice concentration from the University of Bremen ([https://seaice.uni-
72 bremen.de/data/amr2/asi_daygrid_swath/n6250/](https://seaice.uni-bremen.de/data/amr2/asi_daygrid_swath/n6250/)) over a 24 hour analysis run. Then, using the improved initial condition, a
73 66 hour forecast is produced. The operational archive of the model is located at [https://thredds.met.no/thredds/fou-
75 hi/barents25.html](https://thredds.met.no/thredds/fou-
74 hi/barents25.html). In this model, sea ice boundaries were treated as open water until the implementation of the time-varying
76 boundaries described in this work. The model has been run operationally from March 2019 and its results evaluated against
77 observations detailed in 2.4.1.

77 2.1.2 S4K model

78 The S4K (the Svalbard 4km) model has a slightly different domain than the Barents-2.5km model (Fig. 1) and lower horizontal
79 (4 km) and vertical (35 sigma layers) resolution in the ocean, while the configuration of ice categories and vertical
80 discretization is the same as in both setups. The domain covers a slightly different area to allow producing boundary conditions
81 for fjord models in Eastern Greenland. It is based on METROMS coupled with CICE following the same procedure described
82 above for the Barents-2.5 km model (<https://doi.org/10.5281/zenodo.5815093>) (cf. – 2.1.1 and 2.1.3). The ocean and sea ice
83 are forced with atmospheric fields from ECMWF Reanalysis v5 (ERA5, [https://www.ecmwf.int/en/forecasts/dataset/ecmwf-
85 reanalysis-v5](https://www.ecmwf.int/en/forecasts/dataset/ecmwf-
84 reanalysis-v5)). River forcing is based on: ArcticRims (<https://rims.unh.edu>), for Russia and North America, catchment area
86 discharge estimates from the Norwegian Water Resources and Energy Directorate (NVE, <http://nve.no>), for Northern Norway
87 and Mernild and Liston (2012) for Greenland. Sea ice boundary conditions are from TOPAZ4 (Sakov et al., 2012; Xie, 2017)
88 and ocean boundary conditions are from the A4 model (Hattermann et al., 2016). This model was run from August 2014 until
89 July 2015 and its results evaluated against observations detailed in 2.4.2.



90

91 **Figure 1. Barents-2.5 km and S4K model domains. The insert at the right bottom corner represents Svalbard and the area where**
92 **the various drifts (lines showing the begin and end dates of each drift) of the N-ICE2015 expedition (Granskog et al., 2018) took**
93 **place and along which sea ice and ocean data detailed in Table 3 were collected.**



94 **2.2 Coupling between ROMS and CICE**

95 The coupling between ROMS and CICE was implemented at the Norwegian Meteorological Institute using The Model
 96 Coupling Toolkit (MCT, <https://www.mcs.anl.gov/research/projects/mct/>) and creating the METROMS framework mentioned
 97 above (e.g. Fritzner et al., 2019, <https://doi.org/10.5281/zenodo.5067164>). An early version of METROMS was also used by
 98 Naughten et al. (2017; 2018) and the coupling was very briefly described in those papers. ROMS is the controlling software
 99 acting through the drivers CICE_InitMod.F90 and CICE_RunMod.F90 to initialize and run CICE [these drivers are called
 100 from ROMS master routine (master.F)]. The variables exchanged through MCT are detailed in Table 1. The underlying
 101 philosophy behind the coupling is that fluxes are calculated in the model with most details of the underlying process, and then
 102 passed conservatively to the other. Thus, all fluxes except the production of 'frazil ice' are calculated in the ice model. Frazil
 103 ice production is simplified, and it is only assumed implicit in the system. The only variable stored in ROMS is the energy
 104 used to increase ocean temperature to the freezing point of seawater when forcing has produced under-cooled water in ROMS.
 105 This energy deficit is then passed to the ice model (frzmlt variable in Table 1) and converted to a suitable amount of
 106 consolidated ice with heat and salt content consistent with the forcing. Any salt expelled from the ice by this process is then
 107 passed back again to ROMS.

108 Exchange frequency between the models depends on synchronization timestep and must be a common multiple of involved
 109 model timesteps. In default setups the models run concurrently on separate sets of compute cores, with a delayed exchange of
 110 fields, such that information calculated in one component is used in the other at the next coupling time interval. The coupled
 111 variables are declared in both ROMS and CICE and transferred both ways through MCT routines utilizing the underlying MPI
 112 library.

113

114 **Table 1. Data exchange between ROMS and CICE through MCT (see text).**

From ROMS to CICE		From CICE to ROMS	
Name and abbreviation	Dimensions	Name and abbreviation	Dimensions
Sea surface salinity (sss)	psu	Ice concentration (aice)	dimensionless
Sea surface temperature (sst)	°C	Freshwater flux from ice (freshAI)	kg s ⁻¹
Melt-freeze potential (frzmlt)	W m ⁻²	Salt flux from ice (fsaltAI)	kg s ⁻¹
Velocity components (u and v)	m s ⁻¹	Nonradiative heat flux from ice (fhocnAI)	W m ⁻²
Free surface height (ssh)	m	Radiative heat flux through sea ice (fswthruAI)	W m ⁻²



Stress components in x-direction
and y-directions (strocnx and
strocny) N m^{-2}

115

116 2.3 Implementation of time-varying boundary condition in the Los Alamos Sea Ice Model

117 2.3.1 Software details

118 We describe the main code changes in Table 2. We defined a Boolean variable (`sea_ice_time_bry`) that must be set to *True* in
119 the CICE input file (`ice_in`) whenever time-dependent boundary fields are used. The main CICE model drivers
120 `CICE_InitMod.F90` and `CICE_RunMod.F90` were modified. The first one initializes, and the second runs the model. The
121 initialization driver now includes a call to a routine located in the file containing CICE forcing routines (`ice_forcing.F90`) that
122 initializes boundary variables when `sea_ice_time_bry = True`. Similarly, the run driver includes a call to a function to the
123 subroutine in `ice_forcing.F90` that updates the boundary variables at each time step. Updating implies reading boundary fields
124 from boundary files and interpolating them to the model time step. Details on the boundary files are given below.

125 The new boundary variables match CICE variables. They have a prefix corresponding to the name of the corresponding
126 variable in CICE (Table 2) followed by an underscore and the suffix “bry”. We separated the new variables into ice-category-
127 dependent two and three dimensional (2D and 3D) and ice-category-independent (Table 2). 2D variables represent either
128 surface sea ice properties or bulk properties of ice or snow. 3D variables represent properties that vary vertically in the ice or
129 snow and are resolved as a function of the number of ice and snow layers defined for a simulation. The ice-category-dependent
130 variables have a dimension used to store the values of different ice-categories, defined as a function of sea ice thickness. For
131 details on CICE size-categories see Hunke et al. (2015).

132 We allocate to the boundary variables the same dimensions allocated for the matching CICE variables, even though we need
133 to track their values only along the open boundaries. This occupies more memory than necessary, with boundary variable
134 “working” rectangular arrays being filled with zeros except for the boundary cells, but it simplifies the process of scattering
135 variable values among different tiles in a parallel run, since we may reuse CICE data scattering routines. However, as described
136 below, the boundary NetCDF files have only vector arrays and do not require “extra” space as the working arrays (see below).
137 The CICE file with more modifications for the time-varying boundary implementation is `ice_forcing.F90` (Table 2). New
138 routines were created to construct boundary file names, to read these files and to make the necessary time interpolations. Some
139 specific file reading routines were implemented in `ice_read_write.F90` given the format of boundary files (see below). These
140 routines are called from `ice_forcing.F90`.

141 Boundary restoring takes place in file `ice_restoring.F90`, where the boundary values updated in `ice_forcing.F90` are used to
142 modify the corresponding CICE variables using a relaxation time defined in `ice_in` (`trestore`), along the “halo” cells (Hunke et



143 al., 2015) located at the Northern, Southern, Western and Eastern limits of the model domain. These updates occur in the
 144 routine ice_HaloRestore that was modified from its original version. Snow and ice enthalpies are calculated from
 145 corresponding temperatures. In the tests carried out so far we “relaxed” only the halo cells to follow exactly the way CICE
 146 deals with boundary conditions but a more complex treatment involving a relaxation zone may be considered.
 147

148 **Table 2. Summary of main changes in the Los Alamos Sea Ice Model related with the implementation of time-varying boundaries**
 149 (<https://doi.org/10.5281/zenodo.5067164> and <https://doi.org/10.5281/zenodo.5815093>) (see text).

Modified files	Main changes
ice_in	The Boolean sea_ice_time_bry was added to the domain name list. Time-varying boundary code is used when this variable is set to true.
CICE_InitMod.F90	A call to init_forcing_bry - a new subroutine implemented in ice_forcing.F90 (see below) used to initialize the boundaries if the Boolean sea_ice_time_bry is set to true in the model input file (ice_in, see below).
CICE_RunMod.F90	A call to get_forcing_bry - a new subroutine implemented in ice_forcing.F90 (see below) used to update the boundaries from corresponding files if the Boolean sea_ice_time_bry is set to true in the module input file (ice_in).
ice_forcing.F90	<p>New variables were defined to store boundary values. These parallel all model variables updated by the Los Alamos Sea Ice Model in ice_restoring.F90.</p> <p>Ice-category dependent horizontal (2D) variables: aicen_bry (ice concentration), vican_bry, [ice volume per unit area (m)], vsnon_bry [snow volume per unit area (m)], alvln_bry (concentration of level ice), vlvl_n_bry [volume per unit of area of level ice (m)], apondn_bry, (melt pond fraction), hpondn_bry [melt pond depth category (m)], ipondn_bry [mean pond ice thickness (m)], Tsfc_bry [ice/snow surface temperature (°C)].</p> <p>Ice-category dependent and vertically resolved (3D) variables: Tinz_bry [sea-ice inner temperature (°C)], Sinz_bry (sea-ice inner bulk salinity) and Tsnz_bry [snow inner temperature (°C)].</p> <p>Ice-category independent horizontal (2D) variables: uvel_bry and vvel_bry [x (north/south) and y direction (west/east) velocity components (m s⁻¹)]</p> <p>.</p> <p>New routines were created: init_forcing_bry - calculates current year and final year in forcing cycle. boundary_files - constructs boundary file names from current simulated year. boundary_files (and file_year_bry) - constructs boundary file names from current simulated year. get_forcing_bry - calls boundary_data. boundary_data – defines working arrays for boundary variables, call routines to read boundary files and to interpolate variable values to the model time step. read_bry_ice_data_nc - this is an interface with the following procedures: read_bry_ice_data_nc_2D, read_bry_ice_data_nc_3D, read_bry_ice_data_nc_4D, to read boundary values from NetCDF files, according to their dimensions calling routines available in ice_read_write.F90 (see next Table line). interpolate_data_n or interpolate_data_n_layer - interpolate boundary data between two consecutive time steps. The former and the latter are used for ice-category dependent 2D and</p>



	3D variables, respectively. Other variables reuse the “standard” interpolation routine (<code>interpolate_data</code>).
<code>ice_read_write.F90</code>	Three routines (<code>ice_read_nc_bry_2D</code> , <code>ice_read_nc_bry_3D</code> and <code>ice_read_nc_bry_4D</code>) were added to the interface <code>ice_read_nc</code> to read the different types of boundary data (see above).
<code>ice_restoring.F90</code>	<code>ice_HaloRestore</code> - This is where boundary values are restored, using boundary data and a relaxation time scale (<code>trestore</code>) user-defined in the model input file (<code>ice_in</code>).

150

151 Minor adjustments were implemented for Barents-2.5km to enhance reliability for the operational system, particularly to blend
 152 mismatches between the external and internal solutions. In `ice_HaloRestore`, the first physical points as well as the halos are
 153 restored/nudged. Dynamical variables `uvel`, `vvel`, `divu`, `shear`, and `strength` are restored to the neighboring interior point.
 154 Several technical additions address edge cases. Additional grid variables are extrapolated to halo cells (`ice_grid.F90`). Halo
 155 cells are no longer zeroed during multiprocessor communications (`ice_boundary.F90`). Boundary values are restored before
 156 both thermodynamics and dynamics (in `CICE_RunMod.F90`), which is necessary for prescribing boundary values (i.e., when
 157 `trestore=0`).

158 In the S4K model, the only exception in the boundary restoring process is with `uvel` and `vvel`, which are restored as any other
 159 boundary variable when there is sea ice outside the domain, else internal velocities are assumed. This is to guarantee that the
 160 sea ice motion inside the model domain is properly affected by larger scale drift trends in “long-term” simulations (several
 161 months)..

162 2.3.2 Boundary data details

163 The main challenge with the boundary data is the matching between available model output for a larger domain and the data
 164 needs of CICE. In the examples provided here we used data from TOPAZ4 as explained above. The available outputs relevant
 165 for CICE boundaries include daily values for: ice concentration, ice and snow thickness, and ice east-west and south-north
 166 velocities. There is no data for ice or snow inner or surface temperatures, or for ice salinity. There is no data of any kind of ice
 167 categories. Therefore, we had to make some assumptions. These will have to be defined for each application depending on
 168 available boundary data. In our case we proceeded as follows:

- 169 1) TOPAZ values located along the boundaries of our domains were interpolated to our grids.
- 170 2) Ice-category-dependent variables were stored in boundary files assuming the same number of categories used in our
 171 runs (5). For each grid point, all values were set to zero, except for the category where available “bulk” ice thickness
 172 belonged.
- 173 3) Surface (skin) snow or ice temperatures (in the absence of snow) were set to air temperatures taken from the
 174 atmospheric forcing files, when air temperature was < 0 , else they were set to a slightly negative value.



- 175 4) Inner snow and ice temperatures were obtained by interpolating between the surface temperature and the freezing
176 water temperature.
- 177 5) Inner ice salinities were calculated to match multiyear and first year ice (MYI and FYI, respectively) profiles
178 described in the literature (Gerland et al., 1999). We assumed that when ice thickness was > 1.5 m it was MYI, else
179 it was FYI. In the case of MYI we used the profiles described in older versions of CICE (Hunke et al., 2015, equation
180 76). In the case of FYI we assumed a “C” shaped profile defined by equation 1 (e.g. Figure 3 of Gerland et al., 1999):

181

$$182 \quad S_i = 19.539Z_i^2 - 19.93Z_i + 8.913 \quad (\text{eq. 1})$$

183

184 Where, S_i is the salinity and Z_i is the fractional depth of layer i – zero at the ice top and 1 at the ice bottom.

185

186 Examples of boundary files may be found at: <https://doi.org/10.5281/zenodo.5798076>

187

188 **2.4 Data used for model evaluation**

189 **2.4.1 Barents-2.5 km model**

190 The data used to evaluate the Barents-2.5km model can be found in Table 3. For this model system, the focus was purely on
191 remote sensing of sea ice concentration. AMSR2 (<https://seaice.uni-bremen.de/sea-ice-concentration/amsre-amsr2/>) is a
192 Microwave product with a spatial resolution of 6.25 km, consisting of continuous sea ice concentration values (SIC) between
193 0 and 1.0 (same as the model). The Norwegian ice charts (Dinessen & Hackett, 2016) have a higher spatial resolution of 1km
194 and are produced manually on the basis of multiple data sources, where the primary source is radar data (SAR). Since the ice
195 charts consist of discrete values, the modeled SIC is categorized as shown in Table 4. For AMSR2, continuous values are
196 applied. The satellite products are interpolated to the model resolution of 2.5 km, using bi-linear interpolation for the ice charts,
197 and nearest neighbor method (same product as used for assimilation) for the AMSR2 products. In the comparison, all $SIC > 0$
198 are included, where land, missing values and open water (in both observations and model) are masked out. This means that the
199 entire ice sheet inside the domain of the model is included in the comparison. The satellite products are available daily, except
200 the Norwegian ice charts, that are only available during working days.

201

202

203

204



205 **Table 3. Datasets used for Barents-2.5km model evaluation. The listed references include links to the repositories where data and**
 206 **details on sampling and data processing can be found.**

Compartment	Variable	Description	References
Sea ice	Ice concentration (dimensionless)	Regional high-resolution sea ice charts Svalbard region	Dinessen & Hackett (2016) https://thredds.met.no/thredds/catalog/mocean/siw-tac/siw-metno-svalbard/catalog.html
		AMSR2 sea ice concentration product from University in Bremen	Spren et al. (2008) https://seaice.uni-bremen.de/data/amr2/asi_daygrid_swat/h/n6250/

207

208

209 **Table 4. Ice concentration values and their categorization used for the Ice charts and Barents-2.5 km model validation.**

Ice concentration values	Re-mapped values
<0.01	0
0.01-0.1	0.05
0.1-0.4	0.25
0.4-0.7	0.55
0.7-0.9	0.80
>0.9	0.95

210

211 2.4.2 S4K model

212 Datasets used for model evaluation are listed in Table 5, with links or citations to the various data sources. These include
 213 ocean, sea ice and snow data. We used satellite products and *in situ* data collected during the N-ICE2015 expedition (Granskog
 214 et al. 2018 and Figure 1). Therefore, more detailed comparisons are given for 2015. We also compare TOPAZ4 reanalysis
 215 (<https://doi.org/10.48670/moi-00007>) with S4K model outputs regarding ocean and sea ice variables listed below and in Table



216 5. Ocean data is used here to evaluate the “context” for the sea ice simulations. It includes vertical profiles obtained with a
 217 CTD and with a microstructure profiler during the N-ICE2015 expedition (Table 5).
 218 We used satellite data of sea ice concentrations, from regional high resolution sea ice charts for the Svalbard region (the same
 219 mentioned above for the Barents-2.5km model), and for sea ice and snow thickness, from the European radar altimeter CryoSat-
 220 2, generated at Alfred Wegener Institute (AWI) for the winter period (October-April) (Hendricks & Ricker, 2020). We also
 221 used Cryosat2-SMOS weekly Arctic sea ice thickness data (Ricker et al., 2017, <https://spaces.awi.de/display/CS2SMOS>).
 222 Sea ice plus snow thickness were collected with a helicopter-borne electromagnetic induction sounding (HEM) (King et al.,
 223 2016) and a ground based electromagnetic instrument (EM31) (Rösel et al., 2016a) with footprints of approximately 50 m and
 224 3-5 m, respectively (Haas et al., 2009). Snow thickness was measured with a magna probe with a footprint of approximately
 225 0.2 m (Rösel, 2016b).
 226

227 **Table 5. Datasets used for S4K model evaluation. The listed references include links to the repositories where data and details on**
 228 **sampling and data processing can be found. CTD – conductivity-temperature-depth; MSS90L – Ocean microstructure profiler;**
 229 **HEM - helicopter-borne electromagnetic induction sounding; EM31 - ground based Electromagnetic instrument.**

Compartment	Variable	Description	References
Ocean	Practical salinity (psu)	N-ICE2015 ship-based CTD and ocean microstructure profiles (MSS90L)	Dodd et al. (2016) and Meyer et al. (2016) for CTD and MSS90L data, respectively.
	<i>In situ</i> temperature (°C)		
Sea ice	Ice concentration (dimensionless)	Regional high-resolution sea ice charts Svalbard region	Dinessen & Hackett (2016)
		Arctic sea ice freeboard and thickness from the European radar altimeter CryoSat-2	Hendricks & Ricker (2020)
	Ice and snow thickness (m)	Cryosat2-SMOS weekly Arctic sea ice thickness data HEM, EM31 and magnaprobe data collected during the N-ICE2015 expedition (Granskog et al., 2018)	Ricker et al. (2017), King et al. (2016) for HEM, Rösel (2016a and b) for EM31 and magnaprobe data, respectively.

230



231 2.5 Model simulations

232 Simulations carried out with the Barents-2.5 km model are short-term, in accordance with its operational nature. Model
233 evaluation was based on idealized simulations and on operational simulations and focused on sea ice concentration, which is
234 the main variable of interest for this model. In the case of the S4K model, ~one-year simulations were carried out and
235 comparisons between model and observations were focused on sea ice concentration, ice and snow thickness. Moreover,
236 comparisons for the oceanic variables were also carried out.

237 2.5.1 Barents-2.5 km model

238 Model experiments with idealized wind forcing have been conducted with the Barents-2.5 km model in order to visually
239 showcase the effects of using time-varying boundary conditions. The model was initialized from TOPAZ4 fields at 2019-09-
240 01 and it ran until 2019-09-20. One run without the time-varying boundaries (just like the operational model ran before) and
241 one with the boundaries extracted from TOPAZ4 results for the same period. All aspects of the model run, except the wind
242 forcing, were realistic. The wind forcing was idealized to be purely in the model xi-direction, positive in the first part of the
243 run and negative in the latter part of the run. The goal was to blow the sea ice away from the left-most boundary before
244 reversing the wind and observe the interaction with the boundary when the sea ice is forced towards it again. More specifically,
245 the wind forcing was:

$$246 U_{wind} = \begin{cases} 10.0 \text{ ms}^{-1}, & t \leq 2019.09.07 \\ -10.0 \text{ ms}^{-1}, & t > 2019.09.07 \end{cases}$$

247
248 We also compare results obtained with operational simulations before and after the time-varying boundaries were introduced.
249 These contrasting results are also evaluated against satellite data. The operational model is initialized with data from TOPAZ4.
250 We began using time-varying boundary conditions in the operational forecasts in October 2019 after spinning up the model
251 for one month.

252 2.5.2 S4K model

253 The model was initialized from TOPAZ4 fields and ran from January 2014 until July 2015. Results were analyzed only from
254 October 2014 after some spin-up time. Model output was compared with observations of ocean and sea ice variables measured
255 in situ during the N-ICE2015 expedition (Granskog et al., 2018). Here we focus only on the evaluation of hydrographical
256 properties with depth and on temperature-salinity diagrams. Satellite data was used for sea ice concentration and sea ice +
257 snow thickness (Table 5). Comparisons were also made with TOPAZ4 results since it is an operational system in use by the
258 Copernicus Marine Service (<https://marine.copernicus.eu/>) and it provides S4K sea ice boundary conditions. Ocean boundary
259 conditions were from the Pan-Arctic A4 model described in Hattermann et al. (2016). The decision of using ocean boundary



260 conditions from one model and sea ice boundary conditions from another one was based on results from preliminary
261 simulations using only TOPAZ4 ocean and sea ice boundaries. The results of these simulations produced an unrealistically
262 weak West Spitsbergen Current and large salinity and temperature ocean biases (not shown). Therefore, we tried using ocean
263 boundaries from the A4 model which led to a significant improvement in our results.

264 3. Results

265 3.1 Barents-2.5 km model

266 3.1.1 Idealized simulations

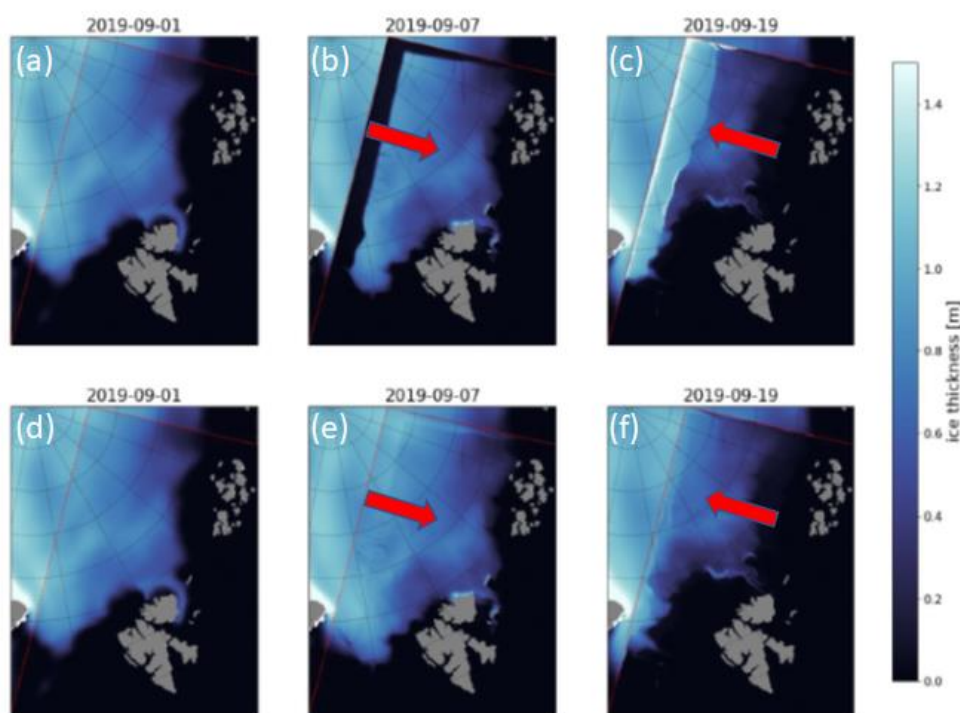
267 The idealized simulations (results available at: <https://zenodo.org/record/4727865#.YOMasRHis2w>) show that when time-
268 varying boundaries are not considered, and the wind direction is perpendicular to one of the boundaries a gap is created between
269 the ice edge of the Barents-2.5 km domain and the boundary with the TOPAZ4 domain. Moreover, when the wind is reversed,
270 ice piles up at the boundary where the gap was formed, artificially increasing sea ice thickness. These “non-realistic” behaviors
271 disappear once time-varying boundaries are considered, resulting in a relatively smooth transition between the results of
272 TOPAZ4 and those of the Barents-2.5 km model (Fig. 2). This transition is not perfect, and signs of a “seam” can be seen
273 where the external fields have been propagating through the boundary.

274 3.1.2 Operational simulations

275 Results from these simulations are available at: <https://zenodo.org/record/4728069#.YOMLDhHis2w>). The upper left panel of
276 Fig. 3 shows typical model sea ice concentration fields prior to the usage of time-varying boundary conditions. While the
277 overall field has a lot of detail in each panel, there are significant artifacts, especially, along the top boundary. Northeastern
278 winds force ice away from the boundary, leaving open water behind (Fig. 3a), creating an artificial polynya in the Barents-2.5
279 km model based on the TOPAZ4 icefields. This was a regular occurrence in the operational model. Fig. 3b shows the day
280 before time-varying boundaries (OBC) were enabled. Here the sea ice field looks more in line with the external model, but
281 local issues along the boundaries are still visible. Fig. 3c shows the day the OBC fields were put into operation. This represents
282 the one-month spun-up fields from TOPAZ4 and immediately exhibits better correspondence with the external fields [note
283 that, at this point, this is a combined effect of the proximity (in time) to the re-initialization from TOPAZ4, and the OBC].
284 Finally, Fig. 3d shows the situation after four months of running with the time-varying boundaries (before AMSR2 assimilation
285 was put into operation). We observe a much better agreement between ice fields of TOPAZ4 and those of Barents-2.5 km
286 models.

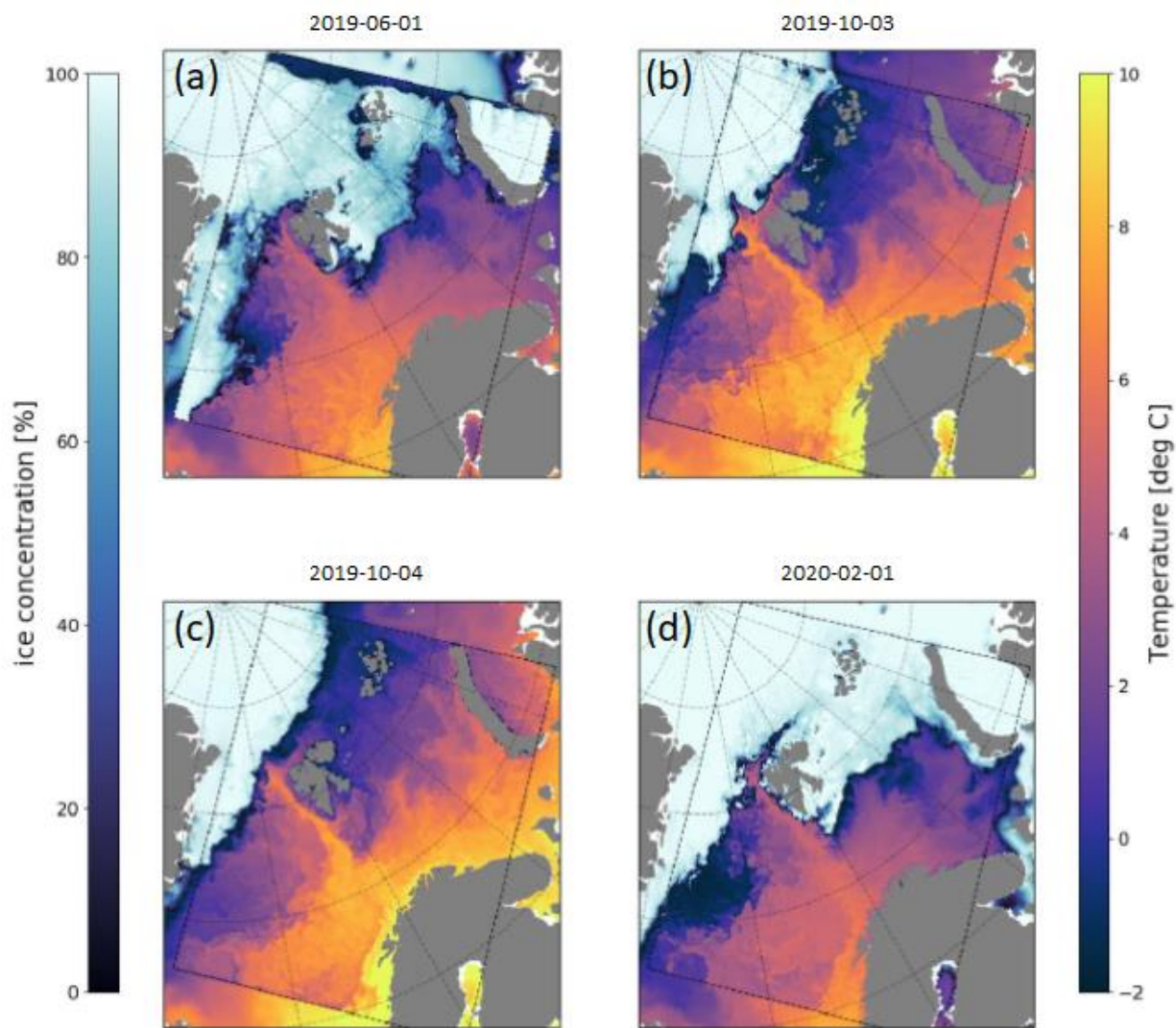


287 The Root Mean Square Error (RMSE) of the predicted sea-ice concentration decreased considerably after the introduction of
288 time-varying boundaries (Fig. 4a). We computed Taylor diagrams (IPCC, 2001; Taylor, 2001), using the MatLab
289 PeterRochford-SkillMetricsToolbox-d7ea0d3 to further analyze the effects. The improvement in model performance was
290 negligible when the daily total sea-ice extent was considered (Fig. 4b). However, a large improvement is apparent when
291 spatially resolved data are compared (Fig. 4c), with higher correlation coefficient and lower RMSE for the simulation with
292 time-varying boundaries. Moreover, the model standard deviation becomes very close to that of the data. Altogether, this shows
293 that the model accuracy improved, and that ice concentration variability is better captured.
294

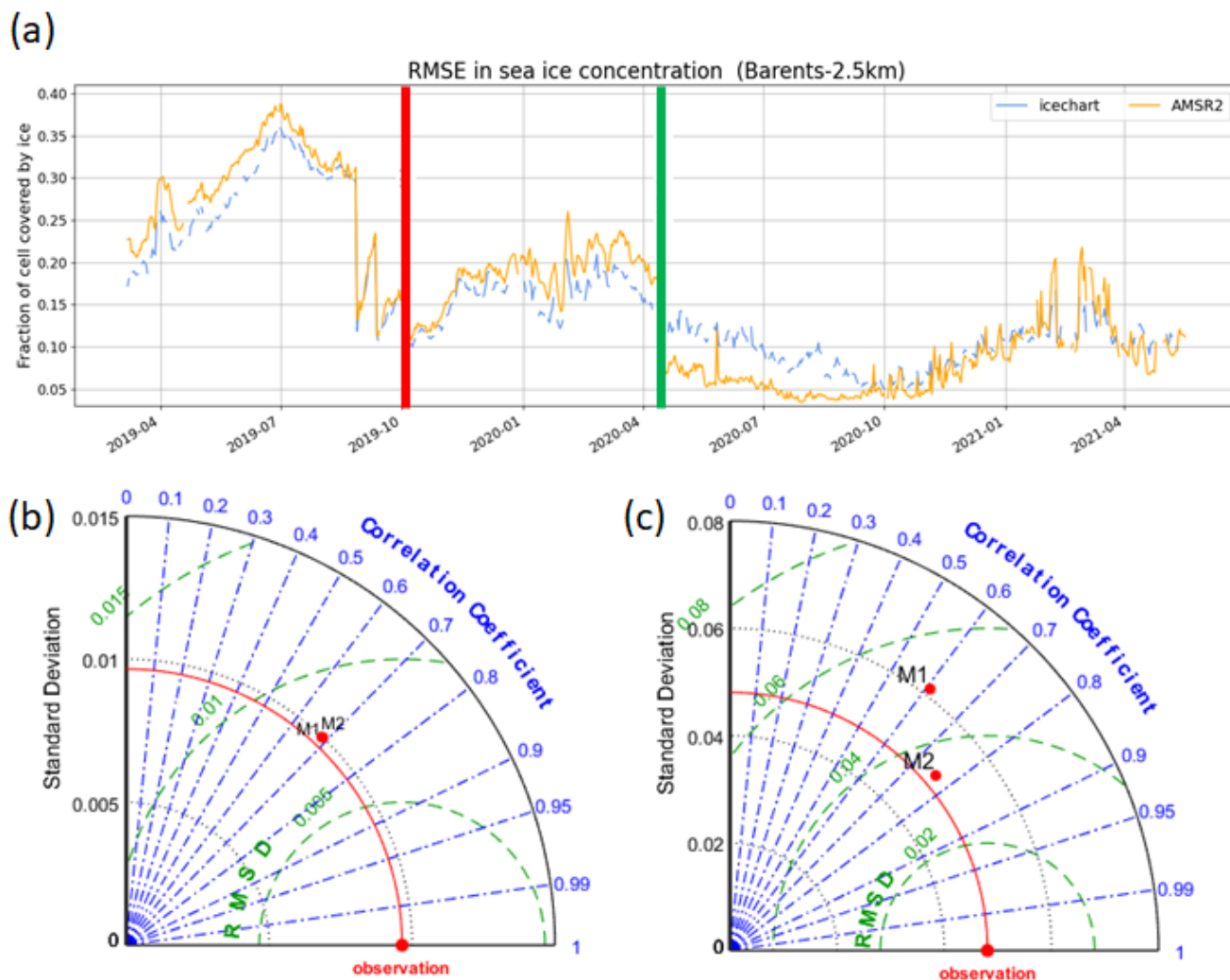


295
296 **Figure 2.** Idealized experiments with the Barents-2.5 km model plotted inside the TOPAZ4 model. Sea ice thickness fields at three
297 moments for the run without (upper row) and with (lower row) time-varying boundaries. The first column is the initial TOPAZ4
298 field interpolated onto the Barents-2.5km grid, the second column corresponds to Barents-2.5 km results after 6 days as the wind
299 turns back in the negative direction, i.e. when the sea ice should be at its maximum displacement relative to the left-most boundary,
300 and the final column shows the state towards the very end of the run when the wind has been blowing “left” for 12 days. Wind
301 direction is shown by the red arrows.

302



303
304 **Figure 3.** Operational simulations with the Barents-2.5 km model, plotted inside the TOPAZ4 model. Sea ice concentration and
305 surface water temperature fields (in the open water areas) are shown for three different dates at 00:00 UTC. The upper and the
306 lower panels correspond to results obtained prior and after the introduction of time-varying boundaries (refer text).



307

308 **Figure 4.** (a) Root Mean Square Error (RMSE) of the Barents 2.5 km model for sea ice concentration, before and after using time-
 309 varying boundaries (vertical red line) and before and after data assimilation began (vertical green line), calculated against AMSR2
 310 and Svalbard ice chart observations (see 2.4.1). Lower panels: Taylor diagrams for the operational Barents-2.5 km simulations and
 311 AMSR2 observations, without (M1) and with (M2) the time-varying boundaries; (b) Daily results averaged over the whole model
 312 domain; (c) spatially resolved daily results. The red line in the Taylor charts depicts the standard deviation of the observations. The
 313 green isolines show the RMSE and the correlation coefficient is shown in blue.

314



315

316 **3.2 S4K model**

317 We present first results for ocean variables and then for sea ice variables. In both cases we compare S4K with TOPAZ4 results
318 and with observations.

319 **3.2.1 Ocean results**

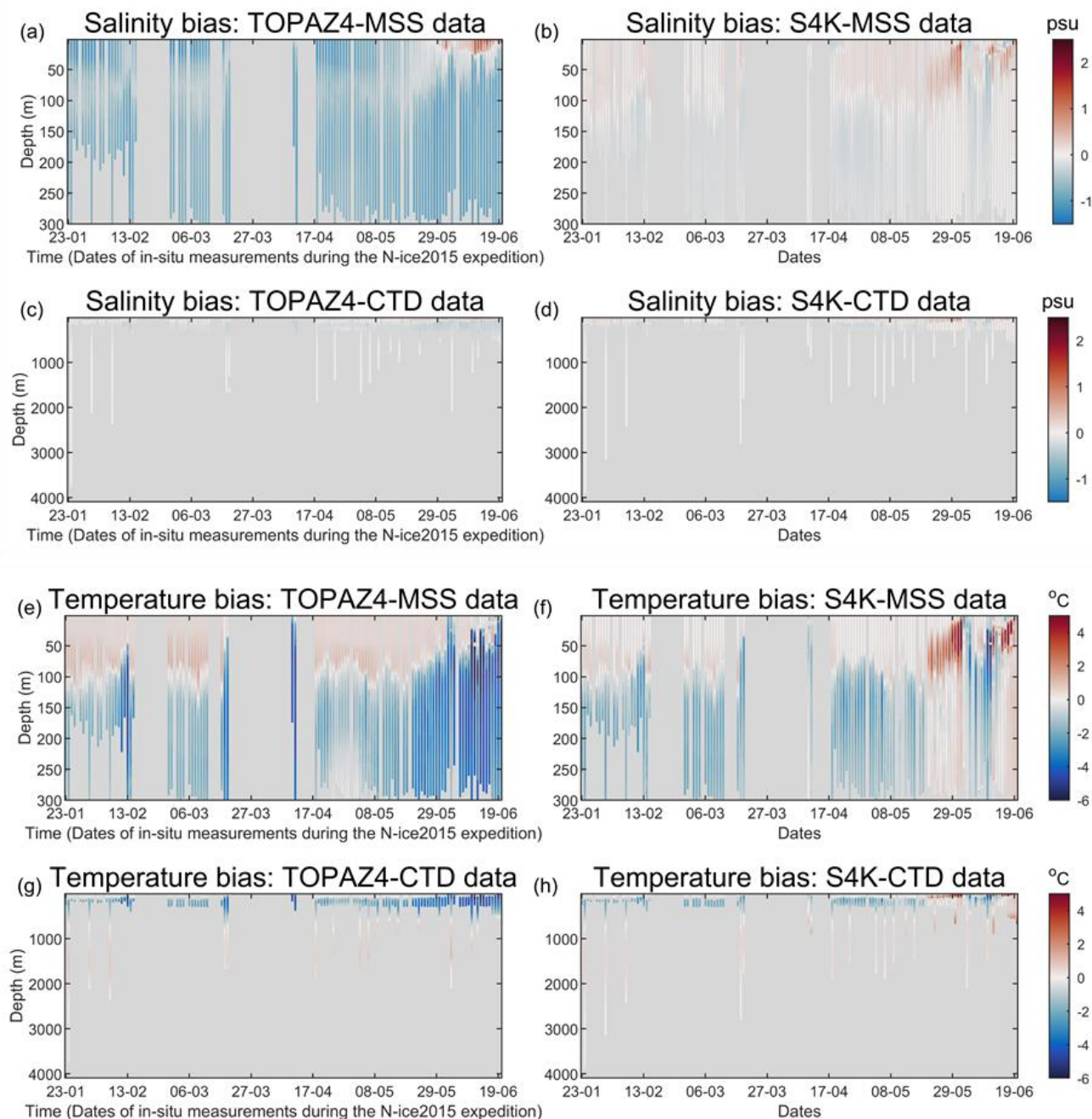
320 TOPAZ4 and S4K model bias for salinity and temperature in 2015 are larger between c.a. 100 and 300 m (Figs 5 and 6).
321 Extreme median salinity and temperature biases are ~ -0.3 and -4 °C and, $\sim +0.2$ and -1.5 °C, for TOPAZ4 and S4K, respectively
322 (Figs. 5 and 6). Temperature-salinity diagrams show better similarity between S4K and observations than between TOPAZ4
323 and observations (Fig. 7).

324 **3.2.2 Sea ice results**

325 Sea ice concentration and sea ice plus snow thickness from satellite products, TOPAZ4 and S4K show similar patterns (Figs.
326 8-10). In Fig. 8e and f, 9d and 10d, we plot S4K fields within a rectangle defined by a dashed line and “surrounded” by
327 TOPAZ4 fields to evaluate the transition from TOPAZ4 forcing to the S4K fields. Boundary effects resulting from forcing
328 S4K with TOPAZ4 sea ice data are not visible in the sea ice concentration plots (Fig. 8e and f) and they are quite smooth in
329 the sea ice+snow thickness plots (Figs. 9d and 10d), with the exception of thinner ice along the North-East boundary in January
330 2015 (Fig. 10d) In some occasions, S4K predicts thin ice south eastwards of Greenland to a larger extent than observed in
331 satellite data, and protruding from the ice flowing along Greenland and out of the Fram Strait (Figs. 8f and 10e). This is neither
332 visible in the satellite data, nor in TOPAZ4 results (Figs. 8 - 10).

333 Sea ice + snow thickness results from S4K model are generally lower than those from satellite products and TOPAZ4 results
334 for the overlapping areas. However, sea ice + snow thickness frequency histograms based on EM31 data (Table 5) overlap
335 more with S4K than to TOPAZ4 (Figure 11a and b). A similar comparison based on HEM data shows similar trends (Figure
336 11c and d). Regarding snow thickness based on Magna probe data, both models have a negative bias (Figure 11e and f).

337 Here we show only a limited number of results due to space constraints. However, monthly averaged map plots of sea ice
338 concentration and sea ice plus snow thickness, from the satellite products listed in Table 5, and from TOPAZ4 and S4K for
339 the period August 2014 - July 2015) may be found at: <https://doi.org/10.5281/zenodo.5800110>.



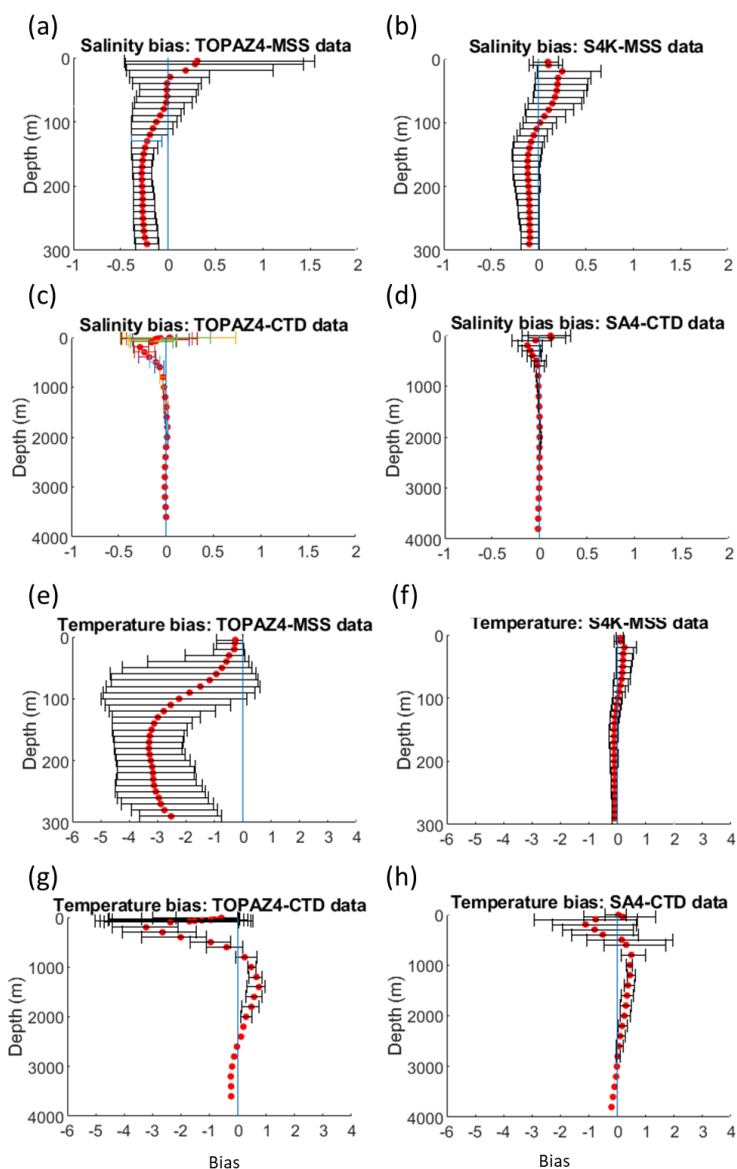
340
341
342
343
344
345

Figure 5. TOPAZ4 [(a), (c), (e) and (g)] and S4K [(b), (d), (f) and (h)] model salinity (upper four panels) and temperature (lower four panels) biases, as a function of time and depth, from profiles obtained during the N-ICE2015 expedition (Granskog et al., 2018). Panels (a), (b), (e) and (f) show biases for the upper 300 m, based on data from ocean microstructure profiles (MSS) (Meyer et al., 2016). Panels (c), (d), (g) and (h) show biases for the whole water column, based on CTD profiles (Dodd et al., 2016) (see Fig. 1, Table 5 and text).



346

347

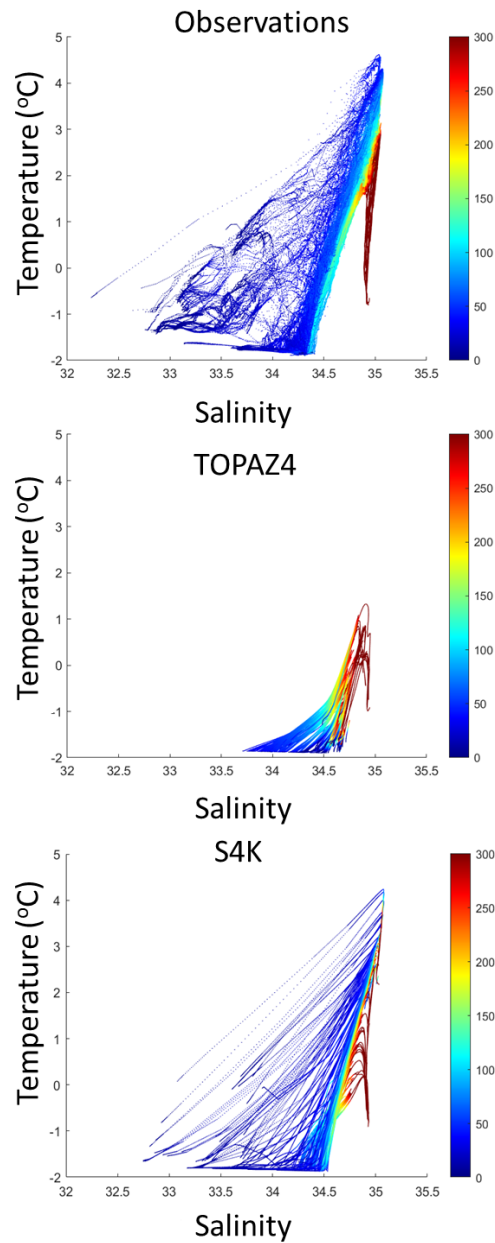


348

349 **Figure 6. Salinity and temperature median bias \pm 10 and 90 percentiles for TOPAZ4 [(a), (c), (e) and (g)] and S4K [(b), (d), (f) and**
350 **(h)], as a function of depth, based on data obtained during the N-ICE2015 expedition (Granskog et al., 2018). Panels (a), (b), (e) and**
351 **(f) show biases for the upper 300 m, based on data from ocean microstructure profiles (MSS) (Meyer et al., 2016). Panels (c), (d), (g)**
352 **and (h) show biases for the whole water column, based on CTD profiles (Dodd et al., 2016) (see Fig. 1, Table 5 and text).**

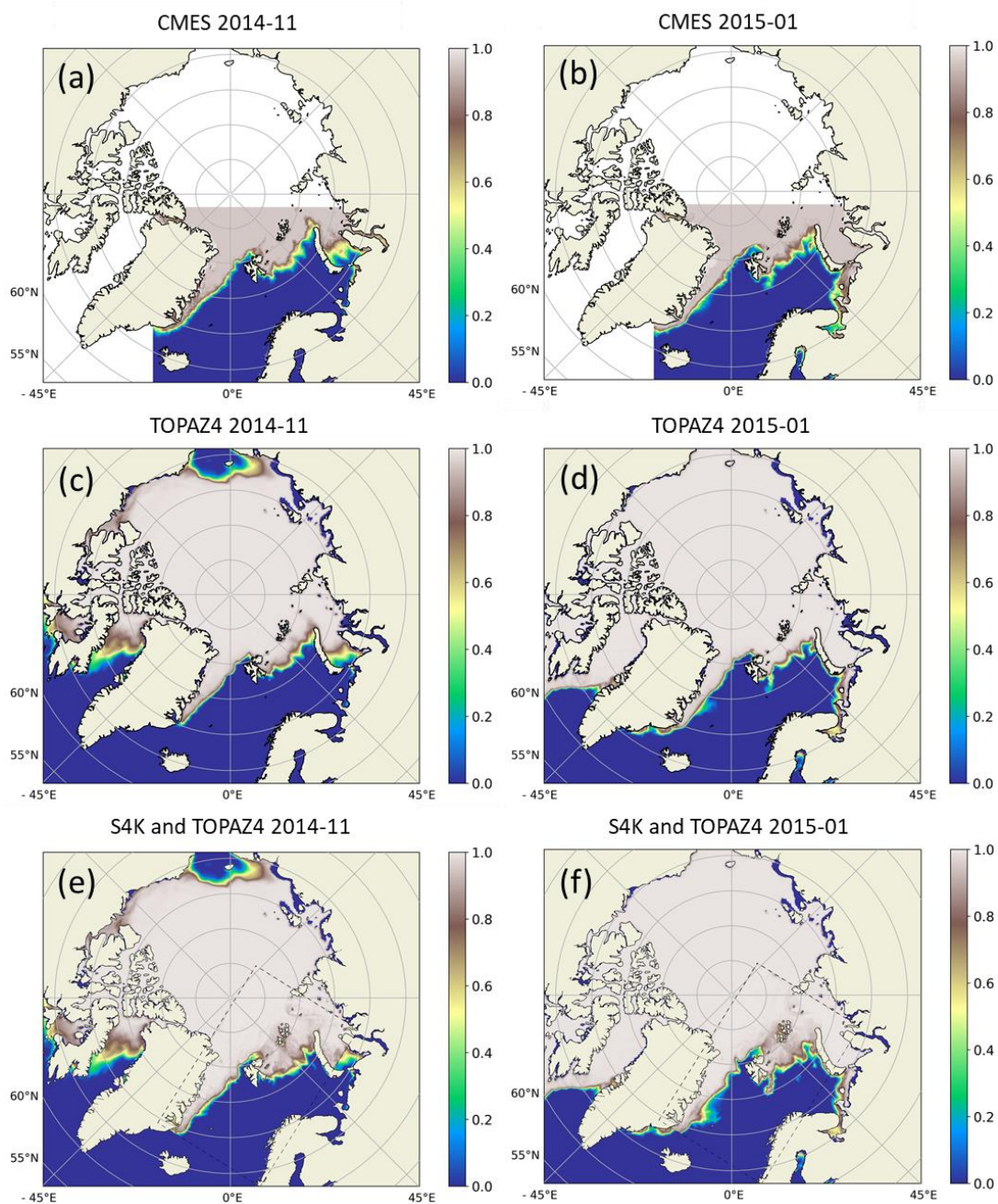


353



354

355 **Figure 7.** Temperature-salinity diagrams for observations collected during the N-ICE2015 expedition (Granskog et al., 2018) (a),
356 TOPAZ4 and S4K models for the same periods and locations as the observations [(b) and (c), respectively]. The color scale represents
357 depth in meters (see Fig. 1, Table 5 and text).



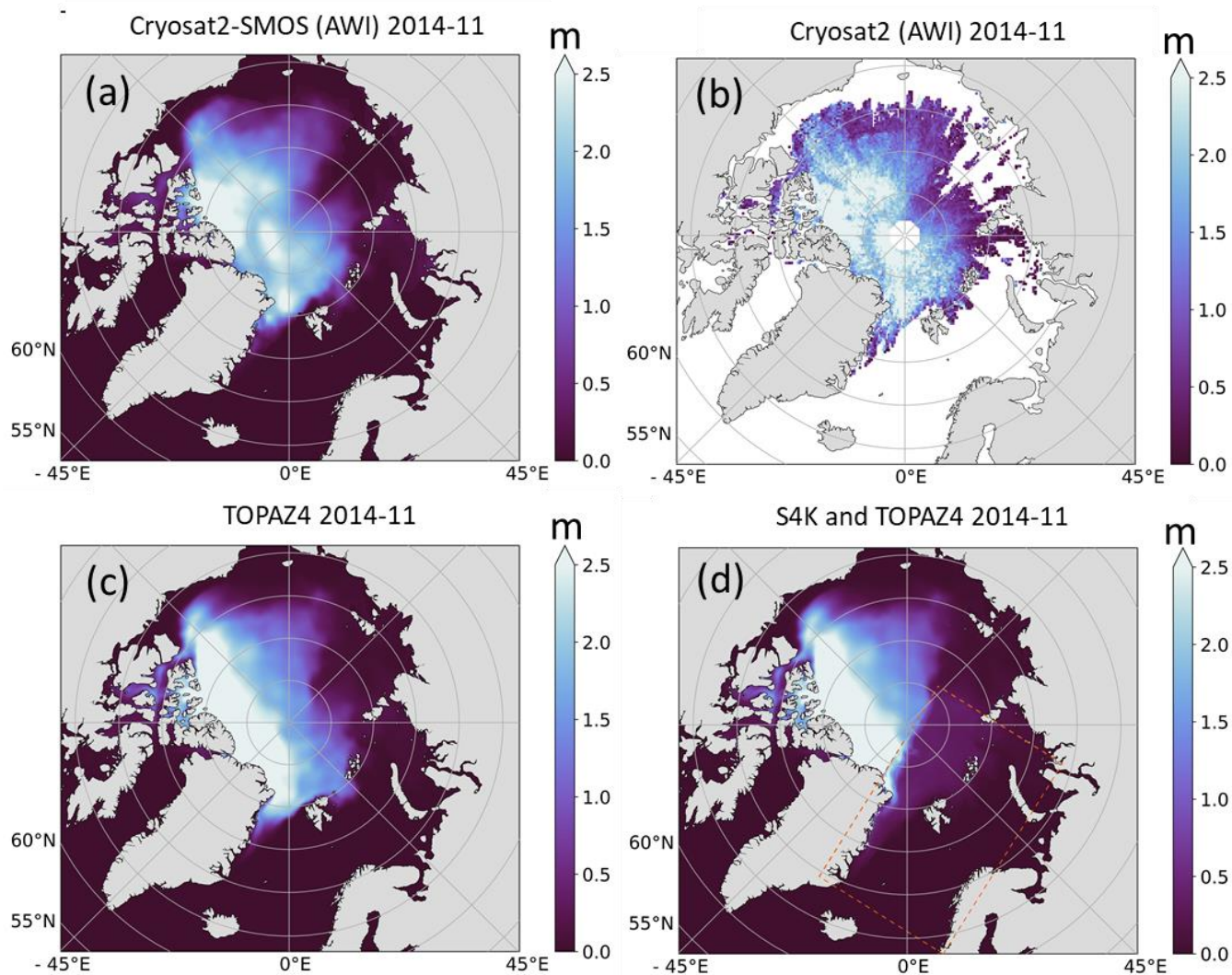
358

359 **Figure 8.** Dinesen & Hackett (2016) CMEMS (SEAICE_ARC_SEAICE_L4_NRT_OBSERVATIONS_011_002) [(a) and (b)],
360 TOPAZ [(c) and (d)] and S4K ((e) and (f)) results for monthly mean sea ice concentration fields for November 2014 (left panels) and
361 January 2015 (right panels). S4K fields are inserted in the TOPAZ4 model domain in the rectangle defined by the dashed line
362 included in panels (e) and (f) (see text).



363

364



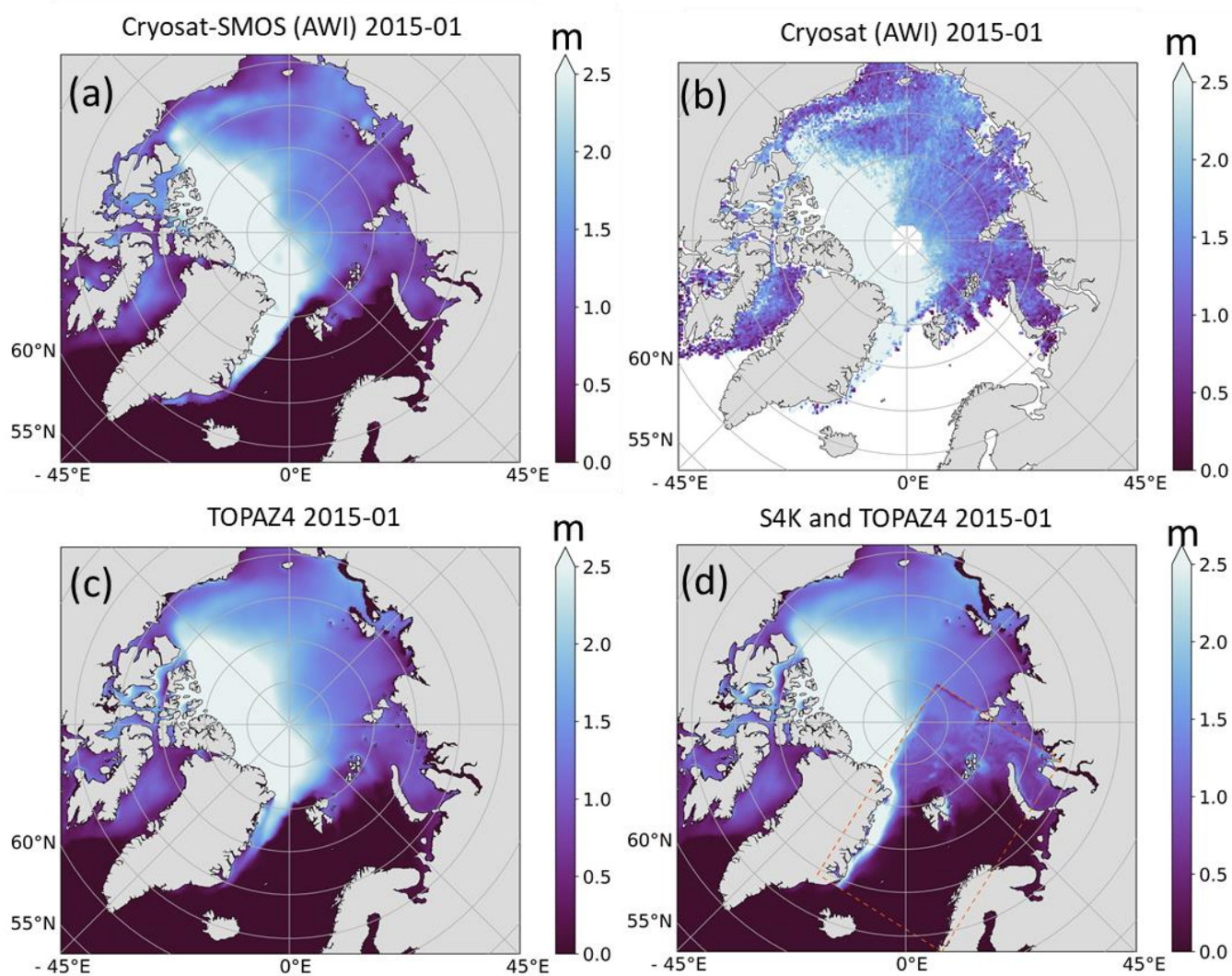
365

366

367

368

Figure 9. Cryosat2-SMOS (a), Cryosat (b), TOPAZ (c) and S4K (d) monthly mean sea ice + snow thickness for November 2014. S4K fields are inserted in the TOPAZ4 model domain in the rectangle defined by the dashed line included in panel (d) (see text).

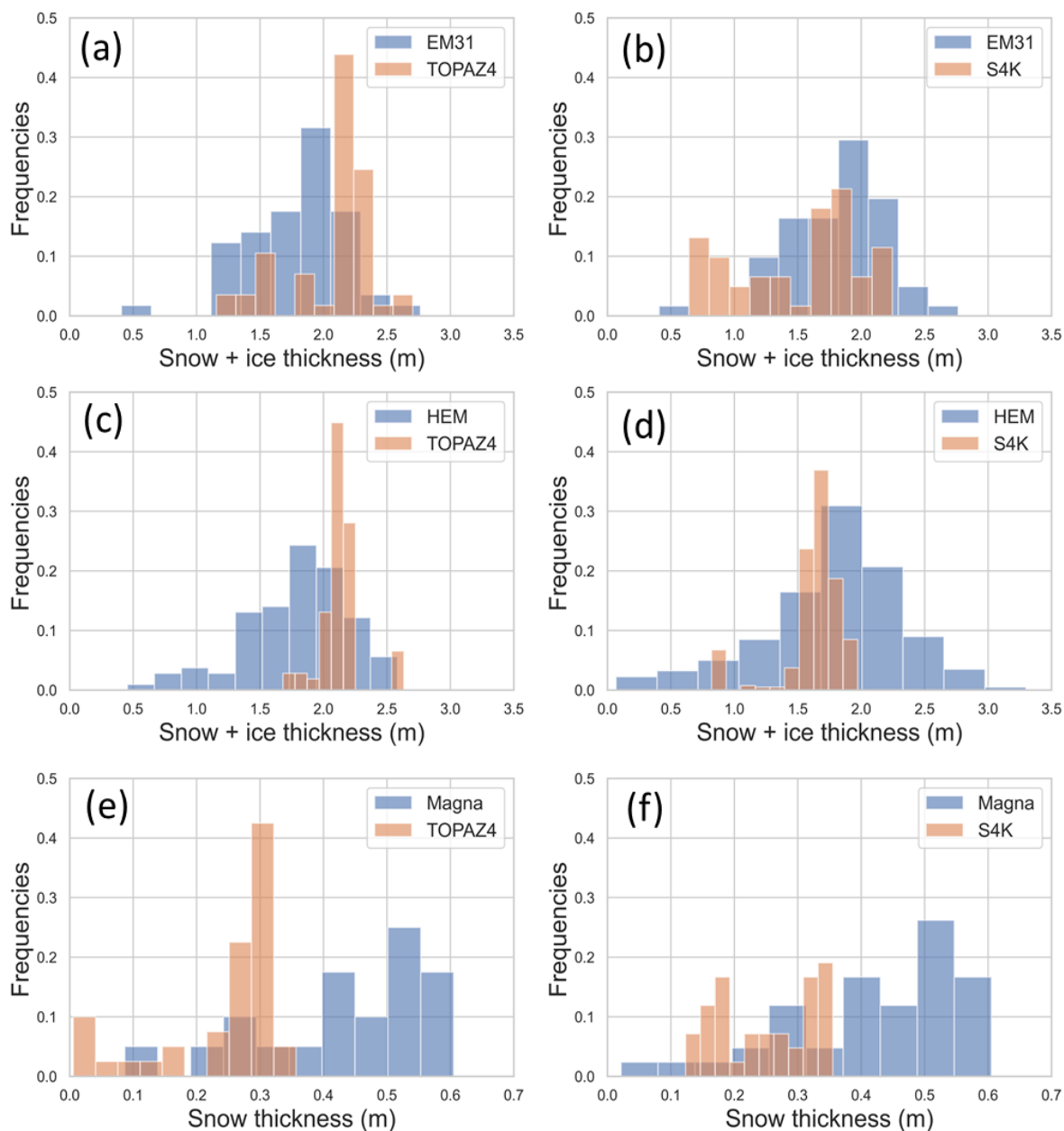


369

370 **Figure 10.** Cryosat2-SMOS (a), Cryosat (b), TOPAZ (c) and S4K (d) monthly mean sea ice + snow thickness for January 2015. S4K
371 fields are inserted in the TOPAZ4 model domain in the rectangle defined by the dashed line included in panel (d) (see text).

372

373



374

375 **Figure 11.** Observed (blue) and modeled (brown) frequency distributions of snow + ice thickness [(a)-(d)] and only snow thickness
 376 [(e) and (f)]. Measurements were taken during the N-ICE2015 expedition with the instruments indicated at the top of the panels:
 377 HEM [(a) and (b)] and EM31[(c) and (d)], for snow + ice thickness and Magna probe [(e) and (f)] for snow thickness. Model results,
 378 averaged for the same areas and days where measurements took place, in the left panels are from TOPAZ4 and, in the right panels
 379 are from S4K (refer Table 5 and text).

380



381

382 4. Discussion

383 The implementation of time-varying boundaries both in the Barents-2.5 km and the S4K models, resulted in a generally smooth
384 transition between the fields of TOPAZ4, providing the boundary conditions, and the fields of the former two models.
385 Moreover, the performance of the operational Barents-2.5 km improved significantly with the usage of time-varying sea ice
386 boundaries. This upgraded performance was also a large contributor to the Barents-2.5km operational forecasts being more
387 widely adopted in downstream applications like drift models, vessel icing models and as support for a specific ship salvage
388 operation near Svalbard.

389 Notwithstanding these results, we still can see some “seams” between the TOPAZ fields and those of the other two models.
390 For example, some ice + snow thickness “artifacts” are visible in the S4K model results, especially in the Northeastern border
391 of its domain (Fig. 10d). These “artifacts” may arise from drift differences inside the domain and at the boundaries. Such
392 artifacts were already noted in the Barents-2.5 km model (refer 3.1.1). Another matching problem is the different horizontal
393 spatial resolutions of TOPAZ4 (12.5 km) and the models described herein (2.5 and 4 km). Perhaps the more likely explanation
394 is the mismatch between available TOPAZ4 sea ice fields and those required by CICE (refer 2.3.2 Model boundary data
395 details). Recall from section 2.3.2 that extensive assumptions had to be made in order to fit the limited TOPAZ4 data for all
396 the boundary variables required by CICE. In fact, experiments (not shown) done with a higher resolution model (500 m
397 horizontal resolution) implemented with CICE, nested in the Barents-2.5km model, and using exactly the same sea ice data of
398 the larger model, did not show any seam but instead, a near perfect transition between both domains. This shows the importance
399 of coordinating the storage of adequate outputs from larger models with the “needs” of regional models. The ideal output from
400 a larger model should include the variables listed in Table 2 (corresponding to the variables defined to store boundary values),
401 use the same sea ice categories of the nested model and the same number of sea ice and snow layers.

402 The S4K model has a smaller ocean temperature and salinity bias than that of TOPAZ4, in the region north of Svalbard, where
403 the N-ICE2015 expedition took place (Granskog et al., 2018). Observed biases are larger at the depth range where Atlantic
404 Water and Modified Atlantic Water are found (Meyer et al., 2017). There is a better fit between TOPAZ4 results and satellite
405 data than those of S4K, which may partly result from the data assimilation process of the former. “Spurious” thin sea ice
406 predicted by S4K south eastwards of Greenland (cf. - 3.2.2 and Figs. 8f and 10e) results from the placement of the front
407 between the inflowing Atlantic Water and the Outflowing Polar Surface Water (e.g. Våge et al., 2018). In the S4K model, this
408 front is not close enough to east Greenland on some occasions, allowing very cold surface water to spread towards Svalbard,
409 with production of some thin sea ice.



410 As a final note we emphasize here the compatibility of the changes described in this study with the most recent versions of the
411 Los Alamos Sea Ice Model (CICE + ICEPACK, <https://github.com/CICE-Consortium>), since the files changed and listed in
412 Table 1 are similar to those of the most recent versions.

413 **Code availability**

414 The software code used in this study for the Barents-2.5 km model may be found at:
415 <https://zenodo.org/record/5067164#.YOMK4hHis2w>.

416 The ocean modeling code is a ROMS branch. Code licensing may be found at:
417 http://www.myroms.org/index.php?page=License_ROMS.

418 The software code used in this study for the SA4 model may be found at: <https://doi.org/10.5281/zenodo.5815093>

419 **Data availability**

420 Results from the Barents 2.5 km model may be found at: <https://zenodo.org/record/4727865#.YOMasRHis2w> and
421 <https://zenodo.org/record/4728069#.YOMLDhHis2w>, for the idealized and for the operational simulations, respectively,
422 described in 2.5.1.

423 Graphical sea ice and snow results from the TOPAZ4 and S4K simulations may be found at:
424 <https://doi.org/10.5281/zenodo.5800110>

425 **Authors contribution**

426 Pedro Duarte made the first version of software changes related to the implementation of time-varying boundaries in the CICE
427 code and ran the simulations with the S4K model.

428 Jostein Brændshøi, Yvonne Gusdal and Nicholas Szapiro implemented, tested and adapted those changes in the Barents-2.5km
429 model and ran the simulations shown in the paper with this operational model.

430 Dmitry Shcherbin performed software development and implemented and tuned the S4K model.

431 Pauline Barras processed and helped analyze S4K model results.

432 Jon Albretsen contributed to the analysis of the S4K model results.

433 Annette Samuelsen provided the boundary conditions from TOPAZ4.

434 Jens Bolding Debernard led and performed the implementation of the CICE-ROMS coupling in METROMS, and contributed
435 to discussions of the OBC implementation in Barents-2.5km model.

436 All authors contributed to the writing of the manuscript.



437
438 **Competing interests**
439 The authors declare that they have no conflict of interest.

440 **Acknowledgements**

441 This work has been supported by the Fram Centre Arctic Ocean flagship project “Mesoscale physical and biogeochemical
442 modelling of the ocean and sea-ice in the Arctic Ocean” (project reference 66200), the Norwegian Metacenter for
443 Computational Science application “NN9300K - Ecosystem modelling of the Arctic Ocean around 440 Svalbard”, the
444 Norwegian “Nansen Legacy” project (no. 276730), the European Union’s Horizon 2020 research and innovation program
445 under grant agreement No 869154 (FACE-IT), and the "Arktis 2030"-programme and the project "Vær- og havvarsling for
446 arktisk miljøberedskap" funded by the Norwegian Ministry of Climate and Environment We acknowledge the usage of
447 CryoSat-2 satellite products from the Alfred Wegener Institute (AWI), publicly available under a Creative Commons
448 Attribution 4.0 International (CC BY 4.0) license and the usage of Cryosat2-SMOS satellite products. The production of the
449 merged CryoSat-SMOS sea ice thickness data was funded by the ESA project SMOS & CryoSat-2 Sea Ice Data Product
450 Processing and Dissemination Service, and data from DATE to DATE were obtained from AWI.

451 **References**

452 Dinessen, F., Hackett, B.; Product user manual for regional high resolution sea ice charts Svalbard region
453 SEAICE_ARC_SEAICE_L4_NRT_OBSERVATIONS_011_002 (version 2.3). Copernicus. [https://cmems-](https://cmems-resources.cls.fr/documents/PUM/CMEMS-OSI-PUM-011-002.pdf)
454 [resources.cls.fr/documents/PUM/CMEMS-OSI-PUM-011-002.pdf](https://cmems-resources.cls.fr/documents/PUM/CMEMS-OSI-PUM-011-002.pdf), 2016.
455 Dodd, P., Meyer, A., Koenig, Z., Cooper, A., Smedsrud, L. H., Muilwijk, M., ... Randelhoff, A.: N-ICE2015 ship-based
456 conductivity-temperature-depth (CTD) data [Data set]. Norwegian Polar Institute.
457 <https://doi.org/10.21334/npolar.2017.92262a9c>, 2016.
458 Fritzner, S., Graverson, R., Christensen, K. H., Rostosky, P., Wang, K. G.: Impact of assimilating sea ice concentration, sea
459 ice thickness and snow depth in a coupled ocean-sea ice modelling system, *Cryosphere*, 13, 491-509, 10.5194/tc-13-491-2019,
460 2019.
461 Gerland, S., Winther, J. G., Orbaek, J. B., Ivanov, B. V. (1999). Physical properties, spectral reflectance and thickness
462 development of first year fast ice in Kongsfjorden, Svalbard. *Polar Research*, 18(2), 275-282,
463 <https://doi.org/10.3402/polar.v18i2.6585>, 1999.



- 464 Granskog, M. A., Fer, I., Rinke, A., Steen, H.: Atmosphere-Ice-Ocean-Ecosystem Processes in a Thinner Arctic Sea Ice
465 Regime: The Norwegian Young Sea ICE (N-ICE2015) Expedition, *J. Geophys. Res.-Oceans*, 123, 1586-1594, doi:
466 10.1002/2017jc013328, 2018.
- 467 Haas, C., L. J., Hendricks, S., Rabenstein, L., Pfaffling, P.: Helicopter-borne measurements of sea ice thickness, using a small
468 and lightweight, digital em system. *Journal of Applied Geophysics*, 67:234–241,
469 <https://doi.org/10.1016/j.jappgeo.2008.05.005>, 2009.
- 470 Hattermann, T., Isachsen, P. E., von Appen, W. J., Albretsen, J., and Sundfjord, A.: Eddy-driven recirculation of Atlantic
471 Water in Fram Strait, *Geophys Res Lett*, 43, 3406-3414, 10.1002/2016GL068323, 2016.
- 472 Hendricks, S. and Ricker, R.: Product User Guide & Algorithm Specification: AWI CryoSat-2 Sea Ice Thickness (version 2.3),
473 <https://epic.awi.de/id/eprint/53331/>, 2020.
- 474 Hunke, E. C., Lipscomb, W. H., Turner, A. K., Jeffery, N., Elliot, S.: CICE: the Los Alamos Sea Ice Model. Documentation
475 and User's Manual Version 5.1. Los Alamos National Laboratory, USA. LA-CC-06-012, 2015.
- 476 IPCC: Climate Change 2001: The Scientific Basis, Contribution of Working Group I to the Third Assessment Report of the
477 Intergovernmental Panel on Climate Change [Houghton, J.T., Y. Ding, D.J. Griggs, M. Noguer, P.J. van der Linden, X. Dai,
478 K. Maskell, and C.A. Johnson (eds.)]. Cambridge University Press, Cambridge, United Kingdom and New York, NY, USA,
479 881 pp. (see http://www.grida.no/climate/ipcc_tar/wg1/317.htm#fig84), 2001.
- 480 Jeffery, N., Elliott, S., Hunke, E. C., Lipscomb, W. H., Turner, A. K.: Biogeochemistry of CICE: The Los Alamos Sea Ice
481 Model, Documentation and User's Manual. Zbge_colpkg modifications to Version 5, Los Alamos National Laboratory, Los
482 Alamos, N. M., 2016.
- 483 King, J., Gerland, S., Spreen, G., Bratrein, M.: N-ICE2015 sea-ice thickness measurements from helicopter-borne
484 electromagnetic induction sounding [Data set]. Norwegian Polar Institute. <https://doi.org/10.21334/npolar.2016.aa3a523>,
485 2016.
- 486 Mernild, S. H. and Liston, G. E.: Greenland Freshwater Runoff. Part II: Distribution and Trends, 1960–2010, *J Climate*, 25,
487 6015-6035, doi: 10.1175/JCLI-D-11-00592.1, 2012.
- 488 Meyer, A., Fer, I., Sundfjord, A., Peterson, A. K., Smedsrud, L. H., Muilwijk, M., ... Kusse-Tiuz, N.: N-ICE2015 ocean
489 microstructure profiles (MSS90L) [Data set]. Norwegian Polar Institute. <https://doi.org/10.21334/npolar.2016.774bf6a>, 2016.
- 490 Meyer, A., Sundfjord, A., Fer, I., Provost, C., Robineau, N. V., Koenig, Z., Onarheim, I. H., Smedsrud, L. H., Duarte, P.,
491 Dodd, P. A., Graham, R. M., Schmidtko, S., and Kauko, H. M.: Winter to summer oceanographic observations in the Arctic
492 Ocean north of Svalbard, *Journal of Geophysical Research: Oceans*, 10.1002/2016jc012391, 2017. Naughten, K. A., Galton-
493 Fenzi, B. K., Meissner, K. J., England, M. H., Brassington, G. B., Colberg, F., Hattermann, T., and Debernard, J. B.: Spurious
494 sea ice formation caused by oscillatory ocean tracer advection schemes, *Ocean Model.*, 116, 108–117,
495 <https://doi.org/10.1016/j.ocemod.2017.06.010>, 2017.



- 496 Naughten, K. A., Galton-Fenzi, B. K., Meissner, K. J., England, M. H., Brassington, G. B., Colberg, F., Hattermann, T., and
497 Debernard, J. B.: Spurious sea ice formation caused by oscillatory ocean tracer advection schemes, *Ocean Model.*, 116, 108–
498 117, <https://doi.org/10.1016/j.ocemod.2017.06.010>, 2017.
- 499 Naughten, K. A., Meissner, K. J., Galton-Fenzi, B. K., England, M. H., Timmermann, R., Hellmer, H. H., Hattermann, T., and
500 Debernard, J. B.: Intercomparison of Antarctic ice-shelf, ocean, and sea-ice interactions simulated by MetROMS-iceshelf and
501 FESOM 1.4, *Geosci. Model Dev.*, 11, 1257–1292, <https://doi.org/10.5194/gmd-11-1257-2018>, 2018.
- 502 Ricker, R., Hendricks, S., Kaleschke, L., Tian-Kunze, X., King, J., and Haas, C.: A weekly Arctic sea-ice thickness data record
503 from merged CryoSat-2 and SMOS satellite data, *The Cryosphere*, 11, 1607-1623, <https://doi.org/10.5194/tc-11-1607-2017>,
504 2017.
- 505 Rösel, A., Divine, D., King, J. A., Nicolaus, M., Spreen, G., Itkin, P., ... Granskog, M. A.: N-ICE2015 total (snow and ice)
506 thickness data from EM31 [Data set]. Norwegian Polar Institute. <https://doi.org/10.21334/npolar.2016.70352512>, 2016a.
- 507 Rösel, A., Polashenski, C. M., Liston, G. E., King, J. A., Nicolaus, M., Gallet, J., ... Granskog, M. A.: N-ICE2015 snow depth
508 data with Magnaprobe [Data set]. Norwegian Polar Institute. <https://doi.org/10.21334/npolar.2016.3d72756d>, 2016b.
- 509 Sakov, P., Counillon, F., Bertino, L., Lisaeter, K. A., Oke, P. R., and Korablev, A.: TOPAZ4: an ocean-sea ice data assimilation
510 system for the North Atlantic and Arctic, *Ocean Sci.*, 8, 633-656, doi:10.5194/os-8-633-2012, 2012.
- 511 Spreen, G., L. Kaleschke, and Heygster, G.: Sea ice remote sensing using AMSR-E 89-GHz channels, *J. Geophys. Res.*, 113,
512 C02S03, doi:10.1029/2005JC003384, 2008.
- 513 Taylor, K.E.: Summarizing multiple aspects of model performance in a single diagram. *J. Geophys. Res.*, 106, 7183-7192, 2001
514 (also see PCMDI Report 55, <http://www.pcmdi.llnl.gov/publications/ab55.html>)
- 515 Våge, K., Papritz, L., Havik, L., Spall, M. A., and Moore, G. W. K.: Ocean convection linked to the recent ice edge retreat
516 along east Greenland, *Nat Commun.*, 9, Artn 1287, doi: 10.1038/S41467-018-03468-6, 2018.
- 517 Wei, T., Yan, Q., Qi, W., Ding, M. H., and Wang, C. Y.: Projections of Arctic sea ice conditions and shipping routes in the
518 twenty-first century using CMIP6 forcing scenarios, *Environ Res Lett.*, 15, ARTN 104079, doi:
519 10.1088/1748-9326/abb2c8, 2020.
- 520 Xie, J., Bertino, L., Counillon, F., Lisaeter, K. A., and Sakov, P.: Quality assessment of the TOPAZ4 reanalysis in the Arctic
521 over the period 1991–2013, *Ocean Sci.*, 13, 123–144, <https://doi.org/10.5194/os-13-123-2017>, 2017.

522
523
524
525